



Cite this: DOI: 10.1039/c9cp06802c

Strategy used to synthesize high activity and low Pd catalyst for Suzuki coupling reaction: an experimental and theoretical investigation†

 Xiao Yan,^{‡,ab} Yafei Luo,^{‡,b} Wei Liu,^a Li Liang,^a Ya Gan,^a Zhongzhu Chen,^b Zhigang Xu,^b Hua Wan,^c Dianyong Tang,^{ib,*b} Hubing Shi^{*d} and Jianping Hu^{ib,*a}

Unveiling the reaction mechanism is significant for developing high-performance catalysts. In this paper, a series of precisely controlled Pd_xM_{147-x} (M = Cu, Pt, Au, Rh, Ru) dendrimer encapsulated nanoparticles (DENS) has been successfully synthesized. The mechanisms of Pd_xM_{147-x} as catalysts for Suzuki cross-coupling reactions were investigated by combining experimental and theoretical methods. The experimental results indicate that Pd₇₄Cu₇₃ DEN shows similar activity to Pd₁₄₇ DEN and excellent substrate adaptability under mild reaction conditions. Moreover, the Cu component can play an important role in tuning the catalytic activity of Pd_xCu_{147-x} DEN. Density functional theory (DFT) calculations illustrate that the similar activities of the Pd₁₄₇ and Pd₇₄Cu₇₃ DENs originate from the comparable energy barriers of the rate-determining steps. The partial density of states (PDOS) and electron density differences demonstrate that Cu decreases the intensities of the valence orbitals of the top and edge Pd atoms and weakens orbital interactions between the intermediates and Pd₇₄Cu₇₃ DEN, leading to low desorption energies of the products. This work can provide a promising strategy to reduce the cost of Pd catalysts in Suzuki cross-coupling reactions.

 Received 18th December 2019,
 Accepted 19th February 2020

DOI: 10.1039/c9cp06802c

rsc.li/pccp

1. Introduction

Suzuki coupling, as an efficient C–C cross-coupling reaction, has attracted extensive attention in the field of organic synthesis,^{1,2} and has emerged as a widely used tool for forming C–C bonds. During the past decades, numerous homogeneous catalysts^{3–6} have been developed for palladium complex-catalyzed carbon–carbon cross-coupling reactions. Although the developed homogeneous catalysts possess high stability, easily accessible properties⁷

and controlled reactivity *via* employing various ligands,⁸ many drawbacks are also found, including the lack of recyclability, difficulty of product separation and metal contamination of the product.

The reasonable heterogenization of homogeneous catalysts can efficiently overcome these drawbacks,^{5,9,10} which has stimulated the development of heterogeneous catalysts for C–C cross-coupling reactions.^{11–19} El-Shall and co-workers reported the development of a new family of highly active Pd nanoparticle catalysts supported on partially reduced graphene oxide nanosheets (Pd/PRGO).¹⁸ The Pd/PRGO catalyst shows excellent catalytic activity for Suzuki coupling with a turnover number (TON) of 7800 and a remarkable turnover frequency (TOF) of 230 000 h⁻¹ at 120 °C under microwave heating. Khanna *et al.* provided insights into the nature of the interfacial interactions between metal nanoparticles and defect sites on the graphene surface, demonstrating that the cross-coupling reactions occur at the catalyst surface.¹² Subsequently, they provided a fundamental understanding of how a graphene support may activate both oxidative and reductive reaction steps in the catalytic cycle of Suzuki–Miyaura palladium-catalyzed cross-coupling reactions *via* employing computational and experimental investigations.¹⁵ These studies are significant for designing high-performance heterogeneous catalysts for C–C cross-coupling reactions. However, there is a crucial problem with the heterogenization of homogeneous catalysts; that is, the question of the

^a College of Pharmacy and Biological Engineering, Sichuan Industrial Institute of Antibiotics, Key Laboratory of Medicinal and Edible Plants Resources Development of Sichuan Education Department, Chengdu University, Chengdu 610106, P. R. China. E-mail: hjpcdu@163.com

^b Collaborative Innovation Center of Targeted Therapeutics and Innovation, Chongqing Key Laboratory of Kinase Modulators as Innovative Medicine, Chongqing Engineering Laboratory of Targeted and Innovative Therapeutics, International Academy of Targeted Therapeutics and Innovation, Chongqing University of Arts and Sciences, Chongqing 402160, P. R. China. E-mail: tangdy2008@163.com

^c College of Mathematics and Informatics, South China Agricultural University, Guangzhou 510642, P. R. China

^d Laboratory of Tumor Targeted and Immune Therapy, Clinical Research Center for Breast, West China Hospital, Sichuan University, Chengdu 610041, P. R. China. E-mail: shihb@scu.edu.cn

† Electronic supplementary information (ESI) available. See DOI: 10.1039/c9cp06802c

‡ These authors contributed equally to this work.

high cost of Pd cannot be avoided. Moreover, compared with homogeneous catalysts, heterogeneous catalysts generally exhibit lower turnover numbers and consume larger quantities of precious metal.¹³ Therefore, in order to reduce the cost of Pd catalysts, adding earth-abundant and less expensive transition metals to Pd catalysts is a promising strategy.

According to previous investigations,^{20–27} there is a feasible method that can be employed to reduce the cost of Pd catalysts; that is, the synthesis of Pd-based bimetallic nanoparticles (NPs) in place of pure Pd as a C–C cross-coupling catalyst. Due to the tunable properties and synergistic effects,^{28–30} bimetallic catalysts can exhibit promising prospects as potential alternative catalysts. In general, compared to monometallic NPs, bimetallic NPs may possess much higher catalytic activities, which can be attributed to the advantageous combination of properties. For example, Gao and co-workers synthesized high-performance Pd-based alloy nano-catalysts for the direct synthesis of H₂O₂, combining density functional theory (DFT) calculations and Sabatier analysis.³¹ This study indicated that the valence electrons of Pd-shell atoms could be adjusted to the optimal range to enhance the activity and selectivity of the nanocluster simultaneously *via* introducing dopants with suitable electronegativity. Shishido *et al.* reported that monometallic Pd and Au catalysts were totally ineffective, however Pd–Au alloy nanoparticle catalysts with a low Pd/Au molar ratio showed high activity.³² To sum up, it is necessary to design novel Pd-based bimetallic NPs as C–C cross-coupling catalysts to reduce the cost of Pd catalysts and improve the turnover number.

For C–C cross-coupling, however, so far there is a lack of systematic exploration of the activities of Pd-based bimetallic NPs. It is not clear if there is a trend in Pd-based bimetallic NPs when the second component metal is in the same row or line in the periodic table of the elements. In order to reach this goal, in this investigation, a series of highly dispersed and random component Pd-based bimetallic NPs, namely Pd_xM_{147–x}, M = Pd, Pt, Au, Rh, Ru, Cu, were synthesized. The activities of these bimetallic NPs and the mechanisms of C–C cross-coupling reactions are unveiled in detail by combining experimental studies and density functional theory (DFT) calculations. By performing this investigation, two scientific questions should be answered. One is that a comparison of activities between Pd_xM_{147–x} and pure Pd₁₄₇ should be illustrated and the relationship between the activity of Pd-based bimetallic NPs and the ratio of the second transition metal should be elucidated. Another is that the differences in the natural properties and activities between Pd_xM_{147–x} and pure Pd₁₄₇ should be expounded by analyzing the electronic characteristics. We hope that this investigation will have a significant influence on the current understanding of heterogeneous catalytic C–C Suzuki coupling reactions and future catalyst designs for this reaction.

2. Experimental

2.1 Chemicals

Poly-amidoamine (PAMAM) dendrimer (G6-OH) was purchased from Weihai CY Dendrimer Technology Co., Na₂PdCl₄ from

Sigma-Aldrich Co., the precursor CuCl₂ from Shanghai Macklin Biochemical Co. Ltd, RuCl₃ from Sigma-Aldrich Co., RhCl₃ from Aladdin Co., NaAuCl₄ from Bidepharm Co., and K₂PtCl₆ from Adamas-beta Co. In addition, 4-bromobenzotrifluoride, phenylboronic acid, 4-methoxyphenylboronic acid, 4-trifluoromethylphenylboronic acid, 4-tolylboronic acid, 4-chlorophenylboronic acid and 4-*tert*-butylphenylboronic acid were purchased from Bidepharm Co., 1-bromo-4-nitrobenzene from Innochem Co., 4-bromoacetophenone, 1-bromo-4-*tert*-butylbenzene, 4-bromotoluene and 4-bromoanisole from Energy Chemical Co., and the standard substance biphenyl from Tokyo Chemical Industry Co. All chemicals were used without any purification, and 18 MΩ cm Milli-Q deionized water was employed for all solutions.

2.2 Pd-based NPs synthesis

The G6-OH(Pd_xM_{147–x}) alloy DENs were obtained by the following two-step process:³³ metal ions are first complexed with dendrimers in solution, then reduced by NaBH₄. Here, the synthesis method for G6-OH(Pd₁₄₇) is similar to Crooks' work.³⁴ Briefly, 147 equiv. of freshly prepared 5.88 mM Na₂PdCl₄ stock solution was added to a 2.0 μM solution of G6-OH(Pd₁₄₇) PAMAM dendrimer, and the pH value was adjusted to 3.0 using 0.1 M HCl. The solution was stirred for 30 minutes, and again for 15 minutes after adding a 10-fold excess of NaBH₄ from a 60 mM stock solution. It's worth noting that the NaBH₄ must be freshly prepared, or its reducing capacity will be greatly weakened. The freshly prepared G6-OH(Pd₁₄₇) catalyst was first bubbled with N₂ for 10 min, and then water; unreacted NaBH₄ and other impurities were removed by means of ultrafiltration centrifugation. Then 10-fold deionized water was added to the concentrated solution to remove the salts and impurities. After repeating this step twice, the preparation process of the catalyst was complete.

The synthesis strategy of G6-OH(Pd_xM_{147–x}) is similar to that of G6-OH(Pd₁₄₇), except for the order and time of Mⁿ⁺ ions added to the solution. First, Pd²⁺ ions were added to the solution and stirred for 15 minutes, permitting the complexation of Pd²⁺ to the interior of the dendrimer.³⁵ Then, the pH value was adjusted to 7–8 with dilute aqueous NaOH, favoring the complexation of Mⁿ⁺ to completely form G6-OH(Pd_xM_{147–x}), and also gaining the desired Pd²⁺/Mⁿ⁺ ratio by stirring for another 15 minutes. Finally, a 10-fold excess of NaBH₄ was added from a 60 mM stock solution and stirred for another 15 min. After that, the solution was bubbled with N₂ for 10 min and we think that the colloidal metal is G6-OH(Pd_xM_{147–x}) alloy NPs. It is worth noting that G6-OH(Pd_xM_{147–x}) is not molecular in nature; it represents the nanoparticles mainly distributed at this size which are composed of 147 metal atoms.

2.3 Characterization

UV-vis spectra were acquired using a T9 UV-vis spectrophotometer. Transmission electron microscopy (TEM) and line profile analysis by energy dispersive X-ray spectroscopy of the G6-OH(Pd₇₄Cu₇₃) catalysts were carried out using a JEOL JEM-2100F with an accelerating voltage of 200 keV. The ¹H NMR (400 MHz) and ¹³C NMR (100 MHz) information of the isolated

product were recorded using a Bruker Avance 400 spectrometer with CDCl_3 as the solvent.

2.4 Computational details

In this study, Pd_{147} and four different configurations of alloy NPs (containing 73 copper atoms and 74 palladium atoms) were established. The SIESTA³⁶ package with Troullier–Martins norm-conserving pseudopotentials and numerical local basis sets were used for all atoms.³⁷ SIESTA has shown excellent performance for medium and large systems. Large-scale atomic simulation with a neural network potential (LASP) package was employed to explore the global potential energy surface.³⁸ The orbital-confining cutoff was determined from an energy shift of 0.010 eV. The energy cutoff for the real space grid was used to represent the density and was set at 150 Ry. The optimized double- ζ plus polarization (DZP) basis set^{39,40} was employed for all atoms. The lattice constant was set at 28.0 Å to ensure a sufficient vacuum gap between periodic images. The exchange–correlation interactions were described by a generalized gradient approximation (GGA) Perdew–Burke–Ernzerhof (PBE)^{41,42} functional with gamma points. Because the investigated complexes are large-sized molecules, dispersion terms were introduced through the D2 formulation.⁴³ The quasi-Newton L-BFGS method was used for geometry relaxation until the maximal force on each relaxed atom was less than 0.05 eV Å⁻¹. The transition state search adopted the double-ended surface walking method.^{44,45}

3. Results and discussion

3.1 Particle synthesis and characterization

As described in the Pd-based NPs synthesis section, $\text{G6-OH}(\text{Pd}_{147})$; $\text{G6-OH}(\text{Pd}_{74}\text{Cu}_{73})$; $\text{G6-OH}(\text{Pd}_{74}\text{Ru}_{73})$; $\text{G6-OH}(\text{Pd}_{74}\text{Rh}_{73})$; $\text{G6-OH}(\text{Pd}_{74}\text{Pt}_{73})$ and $\text{G6-OH}(\text{Pd}_{74}\text{Au}_{73})$ were synthesized and characterized. The UV-vis absorption spectra are shown in Fig. 1 and Fig. S1 (ESI[†]). $\text{G6-OH}(\text{Pd}_{147})$ and $\text{G6-OH}(\text{Pd}_{74}\text{Cu}_{73})$ show significant differences in the synthesis process. The $\text{G6-OH}(\text{Pd}_{147})$ and $\text{G6-OH}(\text{Pd}_{74}\text{Cu}_{73})$ DENs were prepared *via* first complexing 147 equiv. of PdCl_4^{2-} and 74 equiv. of PdCl_4^{2-} or 73 equiv. of Cu^{2+} to the interior of the dendrimer, respectively. The UV-vis spectra of these precursors exhibit strong absorption bands at ~ 230 and ~ 280 nm and an isosbestic point at ~ 260 nm (Fig. 1, red and green lines). The corresponding peaks originate from the ligand-to-metal charge transfer (LMCT) bands associated with the dendrimer/metal-ion complexes.⁴⁶ The presence of an isosbestic point may imply that all Pd^{2+} ions have been complexed with the dendrimer interior because Pd^{2+} ions are not associated with the dendrimer absorbed in this region interior, which is consistent with Crooks previously published results.⁴⁷ Like the $\text{G6-OH}(\text{Pd}^{2+})_{147}$ complexes, there are LMCT bands at ~ 230 and ~ 280 nm for the $\text{G6-OH}((\text{Pd}^{2+})_{74}(\text{Cu}^{2+})_{73})$ precursors.⁴⁸

After reduction of the $\text{G6-OH}(\text{Pd}^{2+})_{147}$ complex, the LMCT band disappears and the broad-band absorption associated with the nanoparticles is observed (blue line).⁴⁹ It indicates that the additional NaBH_4 added yields monometallic NPs which contain an average of 147 atoms: $\text{G6-OH}(\text{Pd}_{147})$. However, following

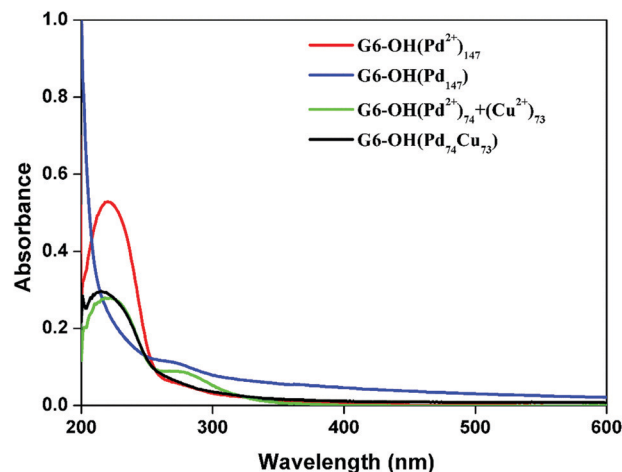


Fig. 1 UV-vis absorption spectra of $\text{G6-OH}(\text{Pd}^{2+})_{147}$ and $\text{G6-OH}((\text{Pd}^{2+})_{74}(\text{Cu}^{2+})_{73})$ complexes before and after reduction with NaBH_4 , with 2.0 μM G6-OH blank.

chemical reduction of the $\text{G6-OH}(\text{Pd}^{2+})_{74}(\text{Cu}^{2+})_{73}$ complexes, the LMCT bands were replaced by broad, monotonically decreasing bands. These characteristic absorption peaks agree with Rothe's results and are attributed to the interband transitions of spherical metal nanoparticles.⁵⁰ Similar results are also found for the reduction of $\text{G6-OH}((\text{Pd}^{2+})_{74}(\text{Rh}^{3+})_{73})$; $\text{G6-OH}((\text{Pd}^{2+})_{74}(\text{Pt}^{2+})_{73})$; $\text{G6-OH}((\text{Pd}^{2+})_{74}(\text{Ru}^{3+})_{73})$ and $\text{G6-OH}((\text{Pd}^{2+})_{74}(\text{Au}^{3+})_{73})$ (Fig. S1, ESI[†]). The adsorption peaks of $\text{G6-OH}(\text{Pd}_{74}\text{Ru}_{73})$ and $\text{G6-OH}(\text{Pd}_{74}\text{Au}_{73})$ can also be attributed to the interband transitions of spherical metal nanoparticles. Moreover, the reduced $\text{G6-OH}(\text{Pd}_{74}\text{Rh})_{73}$; $\text{G6-OH}(\text{Pd}_{74}\text{Pt})_{73}$; $\text{G6-OH}(\text{Pd}_{74}\text{Ru})_{73}$ and $\text{G6-OH}(\text{Pd}_{74}\text{Au})_{73}$ correspond to previous reports.^{51–55} This proves that $\text{G6-OH}(\text{Pd}_{74}\text{M}_{73})$ was produced.

Taken together, although the UV-vis spectra cannot provide sufficient information to infer structural details of the reduced product, they could reflect the proposed synthetic pathway.

In order to unveil the morphological properties of the Pd_{147} and $\text{Pd}_{74}\text{M}_{73}$ ($\text{M} = \text{Cu}, \text{Pt}, \text{Au}, \text{Rh}, \text{Ru}$) DENs, TEM analyses were performed and the results are shown in Fig. 2 and Fig. S2 and S3 (ESI[†]). The TEM images (Fig. 2 and Fig. S2, ESI[†]) demonstrate that the Pd_{147} and $\text{Pd}_{74}\text{M}_{73}$ ($\text{M} = \text{Cu}, \text{Pt}, \text{Au}, \text{Rh}, \text{Ru}$) DENs are highly dispersive and well-ordered. The corresponding TEM data indicate that the initial Pd_{147} DENs have an average diameter of 1.57 ± 0.2 nm (Fig. 2c), which is consistent with Anderson's experimental data⁵⁶ and the calculated diameter of a 147-atom, closed-shell Pd cuboctahedron. After the replacement of Pd by Cu, Pt and Ru, the TEM analyses (Fig. 2d and Fig. S3, ESI[†]) indicate comparable average diameters of 1.6 ± 0.2 , 1.59 ± 0.2 and 1.59 ± 0.2 nm, respectively. However, when replaced with Au and Rh, the TEM results (Fig. S3, ESI[†]) exhibit an average increase/decrease of 0.7/0.1 nm to 2.27 ± 0.2 and 1.47 ± 0.2 nm, respectively.

Moreover, high-resolution TEM (HR-TEM) was also employed to measure the average lattice spacings of Pd_{147} and $\text{Pd}_{74}\text{M}_{73}$ ($\text{M} = \text{Cu}, \text{Pt}, \text{Au}, \text{Rh}, \text{Ru}$) DENs and the related HR-TEM images are plotted in Fig. 3 and Fig. S4 (ESI[†]). The HR-TEM images

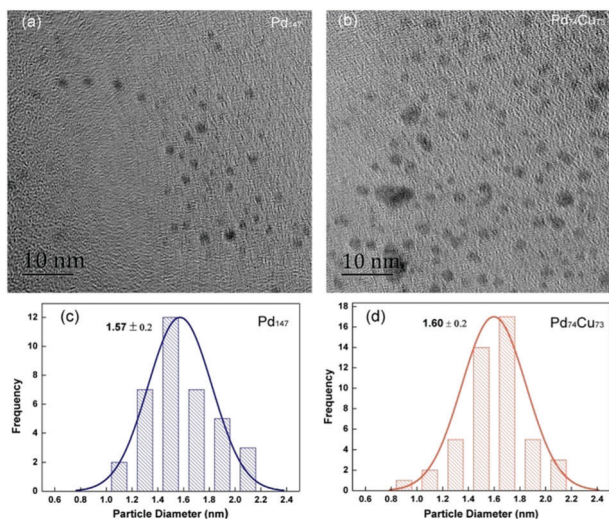


Fig. 2 TEM images of the Pd₁₄₇ (a) and Pd₇₄Cu₇₃ (b) DENs; size distribution histograms of the Pd₁₄₇ (c) and Pd₇₄Cu₇₃ (d) DENs.

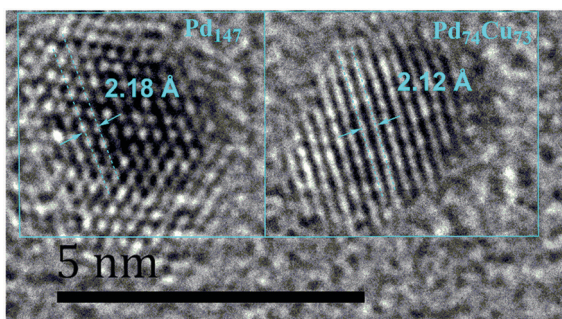


Fig. 3 HR-TEM images of the Pd₁₄₇ and Pd₇₄Cu₇₃ DENs (scale bars = 5 nm).

(Fig. 3 and Fig. S4, ESI[†]) reveal changes in the components of different Pd₁₄₇ and Pd₇₄M₇₃ (M = Cu, Pt, Au, Rh, Ru) DENs. The lattice spacings of 2.18, 2.12, 2.27, 2.26, 2.42, 2.21 Å could be assigned to the same planes of the Pd₁₄₇ and Pd₇₄M₇₃ (M = Cu, Pt, Au, Rh, Ru) DENs. Note that the lattice spacings of the Pd₇₄Pt₇₃ and Pd₇₄Au₇₃ DENs are consistent with Henkelman's⁵⁷ and Xia's work.⁵⁸

Furthermore, with the purpose of unveiling the components of bimetallic Pd₇₄M₇₃ (M = Cu, Pt, Au, Rh, Ru) DENs, energy-dispersive X-ray spectroscopy (EDS) was used and the corresponding images are shown in Fig. 4 and Fig. S5 (ESI[†]). The EDS image in Fig. 4 indicates that Pd and Cu simultaneously exist in the same nanoparticle, demonstrating that the nanoparticle is a Pd–Cu alloy. The atomic ratios of Pd : M are given in Table S1 (ESI[†]); the atomic ratio of Pd : Cu is 52.17% : 47.85%, near the expected atomic ratio of 1 : 1 (74 : 73). Likewise, the EDS images (Fig. S5, ESI[†]) illustrate that the Pd₇₄Pt₇₃, Pd₇₄Rh₇₃, Pd₇₄Ru₇₃ and Pd₇₄Au₇₃ DENs exhibit binary metallic properties. The corresponding atomic ratios of Pd : M (M = Pt, Rh, Ru, Au) are 46.01% : 53.99%, 48.36% : 51.64%, 52.48% : 47.52% and 52.01% : 47.99%; the measured compositions are generally consistent with the expected values.

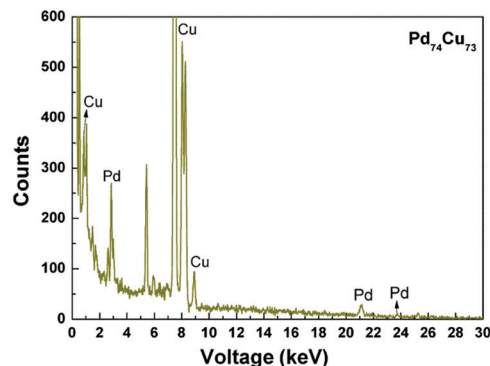


Fig. 4 EDS spectrum of the Pd₇₄Cu₇₃ DENs.

The UV-vis and TEM analyses demonstrate that the Pd₁₄₇ and Pd₇₄M₇₃ (M = Cu, Pt, Au, Rh, Ru) DENs were efficiently synthesized. Besides, the TEM results could provide valuable and useful information for constructing models for theoretical calculation.

3.2 Catalytic activities of Pd₁₄₇ and Pd₇₄M₇₃ (M = Cu, Pt, Au, Rh, Ru) DENs for Suzuki coupling reaction

The catalytic performances of Pd₁₄₇ and Pd₇₄M₇₃ (M = Cu, Pt, Au, Rh, Ru) DENs were initially evaluated for Suzuki coupling of bromobenzene with phenylboronic acid under mild conditions (Fig. 5). Herein, three different evaluation parameters were considered, including HPLC yield (Fig. 5a), turnover number (TON) (Fig. 5b) and turnover frequency (TOF) (Fig. 5c). For the HPLC yield, an external standard method was employed to calculate the product concentration and the corresponding standard concentration curve is shown in Table S2 and Fig. S7 (ESI[†]). The turnover number (TON) and turnover frequency (TOF) were computed *via* the methodology proposed in Karak's⁵⁹ work. The Pd₇₄Cu₇₃ and Pd₁₄₇ DENs were proven to be effective catalysts which displayed HPLC yields of 79.9% and 80.9% after 0.75 h reaction time, TONs of 6389 and 6546, and TOFs of 8519 and 8728 h⁻¹, respectively. Thus, Pd₇₄Cu₇₃ and Pd₁₄₇ DENs

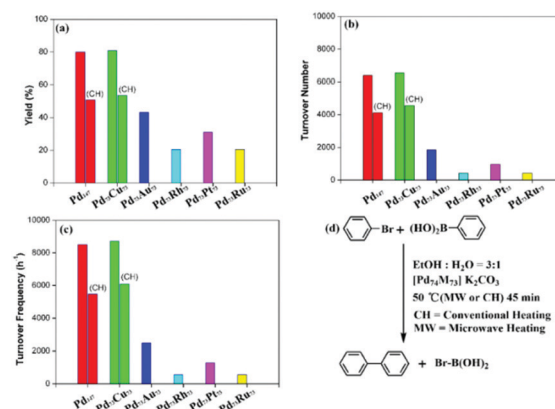


Fig. 5 (a) High performance liquid chromatography (HPLC) yield, (b) turnover number (TON) and (c) turnover frequency (TOF) for the Suzuki cross-coupling reaction catalyzed by Pd₇₄M₇₃ DENs. Except where marked "CH", the source of heat is microwave heating.

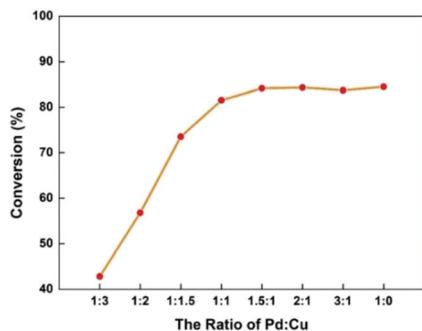


Fig. 6 The conversion rate vs. the Pd:Cu ratio.

outperformed all of the investigated $\text{Pd}_{74}\text{M}_{73}$ ($\text{M} = \text{Pt}, \text{Au}, \text{Rh}, \text{Ru}$) DENs. Moreover, the Pd_{147} and $\text{Pd}_{74}\text{Cu}_{73}$ DENs catalyzed Suzuki cross-coupling reactions by conventional heating were analyzed. Both present high catalytic activity, but at the same time, the reaction yield of microwave heating is higher than that of conventional heating. Obviously, microwave heating could accelerate the reaction,^{60–62} so for this reason microwave heating was used for all the reactions.

To illustrate the role of Cu and further cut the cost of catalytic activity for $\text{Pd}_x\text{Cu}_{147-x}$ DENs, various $\text{Pd}_x\text{Cu}_{147-x}$ DENs were synthesized containing ratios of Pd:Cu = 1:3, 1:2, 1:1.5, 1:1, 1.5:1, 2:1, 3:1 and 1:0. The relationship between the conversion rate for Suzuki coupling and the Pd:Cu ratio in $\text{Pd}_x\text{Cu}_{147-x}$ DENs is elucidated to determine the optimal ratio of Pd:Cu. As shown in Fig. 6, the conversion rate for the Suzuki coupling significantly increases with an increase of the Pd component in $\text{Pd}_x\text{Cu}_{147-x}$ DENs, implying that Pd plays an important role in the catalytic activity. When the Pd:Cu ratio is close to 1:1 (74:73), the catalytic activity of $\text{Pd}_x\text{Cu}_{147-x}$ DENs for the Suzuki coupling nearly reaches the maximum value and the conversion rate is 83%. This result indicates that the activity of $\text{Pd}_x\text{Cu}_{147-x}$ DENs with a Pd:Cu ratio near 1:1 (74:73) is almost equal to that of Pd_{147} DENs for Suzuki coupling. Since the metal Cu is cheaper than Pd, this study can provide an efficient strategy to design low-cost catalysts for Suzuki coupling.

3.3 Catalytic activity of $\text{Pd}_{74}\text{Cu}_{73}$ DENs for Suzuki coupling using various substrates

Bromobenzene and phenylboronic acid modified by electronic-donating groups or electron-withdrawing groups were chosen to investigate whether the $\text{Pd}_{74}\text{Cu}_{73}$ DENs possess high activity for Suzuki coupling. The yields, TON and TOF parameters are given in Table 1. As shown in Table 1, whether the substrates were modified by different electron-donating or electron-withdrawing substituents in the Suzuki coupling, the $\text{Pd}_{74}\text{Cu}_{73}$ DENs still show high catalytic activity, except for the $-\text{CF}_3$ substituent on phenylboronic acid. The reaction times, yields, TONs and TOFs of these Suzuki cross-coupling reactions are 0.75–1.5 h, 32.1–99.9%, 1030–9990 and 687–13 320 h^{-1} , respectively. This demonstrates that the $\text{Pd}_{74}\text{Cu}_{73}$ DENs can effectively catalyze Suzuki coupling using various substrates. Based on these experiments, there was no byproduct generation. Obviously, the homo-coupling pathway can be excluded. However, when phenyl-

Table 1 The catalytic activity of $\text{Pd}_{74}\text{Cu}_{73}$ DENs for Suzuki coupling using various substrates^a

Entry	R	R'	Time (h)	Yield ^b (%)	TON	TOF (h^{-1})
1	H	H	0.75	99.9	9990	13 320
2	CF_3	H	0.75	79.4	6304	8406
3	<i>t</i> -Bu	H	0.75	82.5	8250	11 000
4	CH_3	H	0.75	93.9	8817	11 756
5	CH_3CO	H	0.75	98.4	9683	12 910
6	OCH_3	H	0.75	99.7	9940	13 253
7	NO_2	H	0.75	78.5	6162	8216
8	H	Cl	1.50	95.6	9139	6093
9	H	<i>t</i> -Bu	0.75	99.5	9900	13 200
10	H	CH_3	0.75	94.0	8836	11 781
11	H	CF_3	1.50	32.1	1030	687

^a Reaction conditions: aryl halide (588 μmol), aryl boric acid (588 μmol), 1% mol catalyst, $\text{K}_2\text{CO}_3 = 1.176$ mmol, $\text{EtOH}:\text{H}_2\text{O} = 3:1$ (v/v, 15 mL). The reaction temperature was preset at 50 °C to protect the NPs from high temperature acceleration of aggregation. The reaction was heated by microwave reactor. ^b Isolated yields, ¹H NMR and ¹³C NMR information of the product; see Section S4 in ESI.

boronic acid was modified by an electron-withdrawing group, such as $-\text{CF}_3$, the reaction time was prolonged and the yield, TON and TOF were reduced correspondingly.

3.4 Mechanism of Suzuki cross-coupling reaction and energetic span model analysis catalyzed by Pd_{147} and $\text{Pd}_{74}\text{Cu}_{73}$ DENs

The above experimental results show that the Pd_{147} and $\text{Pd}_{74}\text{Cu}_{73}$ DENs exhibit comparable activity for the Suzuki cross-coupling reaction. To further unveil the inherent factors, the mechanism of the Suzuki cross-coupling reaction was explored in detail with the help of density functional theory (DFT). According to TEM analysis and the previous report,⁶³ the Pd_{147} and $\text{Pd}_{74}\text{Cu}_{73}$ DENs are modeled as cuboctahedron structures in this research. For the $\text{Pd}_{74}\text{Cu}_{73}$ DENs, the Pd:Cu ratio is near 1:1 (74:73) and the distribution of Pd/Cu is uncertain. These alloyed DENs were constructed by randomly assigning each atom to the constituent metals by referring to Henkelman's work.⁶⁴ Table S3 (ESI[†]) shows four configurations of $\text{Pd}_{74}\text{Cu}_{73}$ DENs and the energy differences are no more than 2.0 eV, which means that the $\text{Pd}_{74}\text{Cu}_{73}$ DENs structure may influence the reaction path. As a result, four configurations of $\text{Pd}_{74}\text{Cu}_{73}$ DENs were analyzed. After comparing the energy differences between the $\text{Pd}_{74}\text{Cu}_{73}$ DENs, the adsorptions of bromobenzene on Pd_{147} and $\text{Pd}_{74}\text{Cu}_{73}$ DENs are taken into consideration. As we all know, in the heterogeneous reaction mechanism, the Pd catalysts are mainly distributed on the surface of the Pd NPs, and recent studies point to catalytic recycling taking place at the defect/edge sites of Pd nanoparticles.⁶⁵ For the Pd_{147} DENs, the adsorption of bromobenzene was explored in detail, including at two different top sites and three different bridge sites. The adsorption energies are collected in Table S4 (ESI[†]). As shown in Table S4 (ESI[†]), compared with top adsorption, the adsorptions of bromobenzene at bridge sites possess larger adsorption energies, indicating that bromobenzene is inclined to adsorb on bridge sites. Similarly, for the adsorption of bromobenzene on four different $\text{Pd}_{74}\text{Cu}_{73}$ DENs (*i.e.* configurations

1–4), the stable adsorption configurations can be achieved when the Br and C atoms adsorb on Pd (Table S5, ESI†). The corresponding adsorption energies are -65.9 , -60.4 , -60.8 and -61.2 kcal mol $^{-1}$, respectively.

Based on the above discussion of the adsorption of bromobenzene and phenylboronic acid, the mechanisms of Suzuki coupling are explored by using potential energy profiles (Fig. 7 and Fig. S8, ESI†). As presented in Maseras's work,^{66,67} Suzuki coupling contains three steps, namely oxidative addition, transmetalation and reductive elimination. The oxidative addition process involves cleavage of the C–Br bond of bromobenzene and formation of the C–Pd bond. This step needs to overcome an energy barrier of 12.8 kcal mol $^{-1}$ on Pd₁₄₇ DEN. Nevertheless, for the Suzuki coupling reactions catalyzed by Pd₇₄Cu₇₃ DENs, the oxidative addition process needs to overcome energy barriers of 17.8, 11.8, 23.7 and 25.1 kcal mol $^{-1}$, respectively (for configurations 1–4).

For the transmetalation process, Ph–B(OH)₃[−] first adsorbs on the Pd/Cu atoms of Pd₁₄₇ and Pd₇₄Cu₇₃ DENs to form B–Pd bonds or B–Cu bonds. Two adsorption options are discussed in Fig. 7b. In terms of the adsorption energy, the adsorption of phenylboronic acid on the Pd atoms is more stable than

adsorption on the Cu atoms. Subsequently, the formation of KBr occurs, which is endothermic by about 65.0 kcal mol $^{-1}$ and 60 kcal mol $^{-1}$. Finally, the cleavage of the C–B bond in the adsorbed Ph–B(OH)₃[−] can be achieved *via* TS2. The corresponding energy barriers are 15.4/8.2 kcal mol $^{-1}$, respectively. An interesting phenomenon has been found; when Pd₇₄Cu₇₃ DENs act as the catalyst, the energy barrier of the transmetalation step is reduced from 26.6 to 8.2 kcal mol $^{-1}$. The same results can be obtained for the other three configurations; the energy barriers are 9.7, 15.3 and 23.2 kcal mol $^{-1}$ for configurations 1, 3 and 4. Hence, Cu atoms could cut down the energy barrier of the transmetalation step and accelerate the Suzuki reaction.

Along with the dissociation of B(OH)₃ from the catalyst, the reductive elimination process would lead to the formation of biphenyl *via* TS3 (Fig. 7 and Fig. S8, ESI†). In the case of Pd₁₄₇ acting as the catalyst for Suzuki coupling, the energy barrier of TS3 is 26.6 kcal mol $^{-1}$. Combined with the above investigation, the energy barriers of the transmetalation processes (26.6 kcal mol $^{-1}$) are larger than those of the oxidative addition (12.8 kcal mol $^{-1}$) and reductive elimination processes (25.6 kcal mol $^{-1}$), indicating that the transmetalation process is the rate-determining step for the Suzuki coupling catalyzed by Pd₁₄₇ DENs. As for the energy barriers of Pd₇₄Cu₇₃ DENs, that of reductive elimination is much higher than those of the transmetalation and oxidative addition processes. From the point of view of the energy barriers, an interesting conclusion can be drawn; for Pd₇₄Cu₇₃ DENs (configurations 1, 2, 3, 4) as the catalyst, the rate-determining step for Suzuki coupling is the reductive elimination process. Additionally, once the biphenyl–NPs complex is generated, the complex will be divided into biphenyl and NPs (Pd₁₄₇ and Pd₇₄Cu₇₃ DEN) with largely endothermic energies of 106.2 and 79.2 kcal mol $^{-1}$, respectively. Obviously, Pd₇₄Cu₇₃ DENs acting as the catalyst is more efficient than Pd₁₄₇ DENs in transmetalation processes. What's more, Pd₇₄Cu₇₃ DENs show even better performance than Pd₁₄₇ DENs in the biphenyl desorption process. Presumably, this is the reason why Pd₁₄₇ and Pd₇₄Cu₇₃ DENs exhibit highly similar catalytic activity when the number of catalytic active sites is reduced. This result is supported by reactant conversion, with the reaction times of Pd₁₄₇ and Pd₇₄Cu₇₃ DENs and the TON/TOF relationships with the reaction times illustrated in Fig. S7 (ESI†). Seen from the conversion with reaction times (Fig. S7A and B, ESI†), both Pd₁₄₇ and Pd₇₄Cu₇₃ DENs present nearly the same catalytic activity. Meanwhile, at the first 9 min, the TOF of Pd₇₄Cu₇₃ DENs is much higher than that of Pd₁₄₇ DENs (Fig. S7C and D, ESI†), because the desorption of biphenyl from Pd₁₄₇ DENs is more difficult than from Pd₇₄Cu₇₃ DENs.

By exploring the mechanism of Suzuki coupling and analyzing the energy barriers, it is found that the energy barriers of the rate-determining step are different. This result is consistent with the experimental results; that is, Pd₁₄₇ and Pd₇₄Cu₇₃ DENs exhibit nearly the same catalytic activity.

3.5 Analyses of partial density of states (PDOS) and charge density differences

Herein, the d orbitals of the partial density of states (PDOS) and charge density differences were calculated to expound the

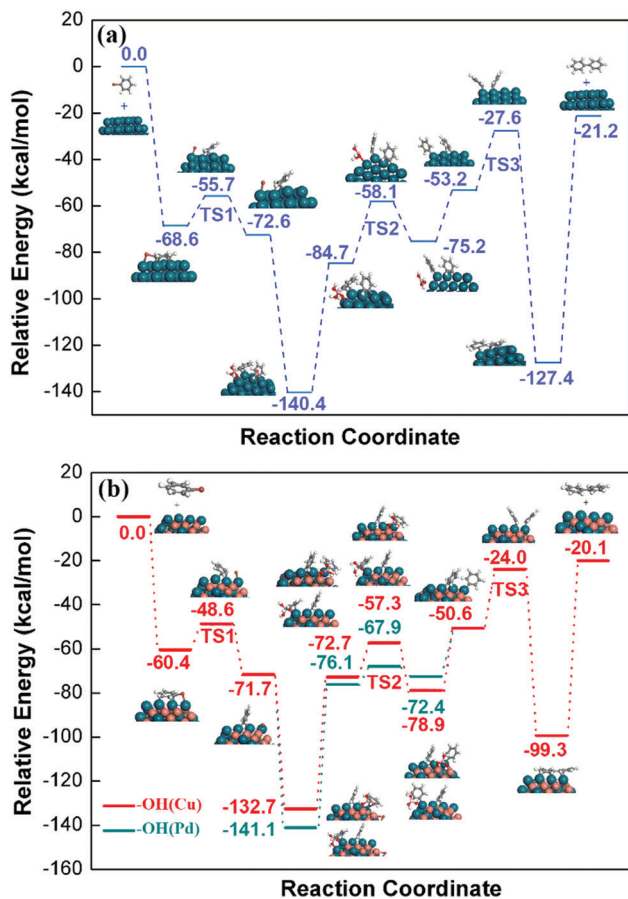


Fig. 7 Potential energy profile of Suzuki cross-coupling reaction catalyzed by Pd₁₄₇ (a) and Pd₇₄Cu₇₃ DENs (b, configuration 2). OH(Cu) means the $-\text{OH}$ of phenylboronic acid adsorbs on the surface of Cu atoms and OH(Pd) means the $-\text{OH}$ of phenylboronic acid adsorbs on the surface of Pd atoms.

similar activity of the Pd₁₄₇ and Pd₇₄Cu₇₃ DENs, the comparable energy barriers of the transmetalation steps and the biphenyl decomposition processes. In this article, the PDOS discussion focuses only on the valence orbitals of the top and edge Pd atoms due to the interactions between the substrate and the catalyst. As plotted in Fig. 8a and d, near the Fermi level, the bands of the top and edge Pd atoms in the Pd₇₄Ru₇₃ (pink line) and Pd₇₄Rh₇₃ (green line) DENs moved to the left, toward the lower energy region, when compared with Pd₁₄₇ DENs; the lower bands lead to lower d-band centers, which are adverse to the adsorption of substrate.^{68–72} For the Pd₇₄Pt₇₃ (blue line) and Pd₇₄Au₇₃ (cyan line) DENs, although the bands of the top and edge Pd atoms are similar to those of Pd₁₄₇ DENs, the intensities of the bands are smaller or larger than those of Pd₁₄₇ DENs. However, in contrast to Pd₇₄Ru₇₃, Pd₇₄Rh₇₃, Pd₇₄Pt₇₃ and Pd₇₄Au₇₃, the bands of the top and edge Pd atoms of Pd₇₄Cu₇₃ DENs are similar to those of Pd₁₄₇ DENs. However, for Pd₇₄Cu₇₃ DENs, the band strengths of the valence orbitals of the top and edge Pd atoms are weaker than those of Pd₁₄₇ DENs near the Fermi level. Therefore, the interactions between the valence orbitals of the top and edge Pd atoms of the Pd₇₄Cu₇₃ DENs with the valence orbitals of the substrate may be decreased, leading to the decrease of adsorption energies (see Fig. 8). This can be

used to explain the reduced desorption energy of biphenyls on Pd₇₄Cu₇₃ alloy NPs.

In addition to the PDOS investigation, the charge density differences were also computed to illustrate the orbital interactions and the results are shown in Fig. 8b and c and Fig. 8e–g. Fig. 8b, c and e show the charge density differences of the transmetalation steps. The charge transfer process can be obtained in this step; phenylboronic acid was activated by base and the charge accumulated around the C and B atoms. Compared with Pd₁₄₇ DENs, the charges accumulate on the surface of C and B atoms more easily and promote the cleavage of the C–B bond; Cu atoms play a charge donor role in this step. Next, the electron density difference plots for the adsorption of biphenyl on Pd₁₄₇ and Pd₇₄Cu₇₃ DENs illustrate the biphenyl decomposition processes (Fig. 8f and g).

Fig. 8f and g show an obvious charge transfer between biphenyl and Pd₁₄₇/Pd₇₄Cu₇₃ DEN. For Pd₁₄₇ DEN, the charges are transferred from Pd₁₄₇ DEN to biphenyl. In contrast, for Pd₇₄Cu₇₃ DEN, the charges are transferred from biphenyl to Pd₇₄Cu₇₃ DEN. The interaction between the d_{z²} orbital of Pd and the p orbital of C leads to the formation of a Pd–C bond. Compared with the Pd₇₄Cu₇₃ DENs, the increased interactions between the d_{z²} orbitals of Pd and the p orbitals of C cause the stronger adsorption of biphenyl on Pd₁₄₇ DENs.

According to the PDOS and electron density difference analyses, compared to the Suzuki cross-coupling catalyzed by Pd₁₄₇ DENs, Cu and Pd have a synergistic effect in the mechanism of the Suzuki cross-coupling reaction catalyzed by Pd₇₄Cu₇₃ DENs (see Fig. 8). It originates from two aspects. One is that Cu can decrease the intensities of the valence orbitals of the top and edge Pd atoms near the Fermi level. Another is that Cu plays a charge donor role in the transmetalation process, leading to weak orbital interactions between the intermediates and Pd₇₄Cu₇₃ DENs.

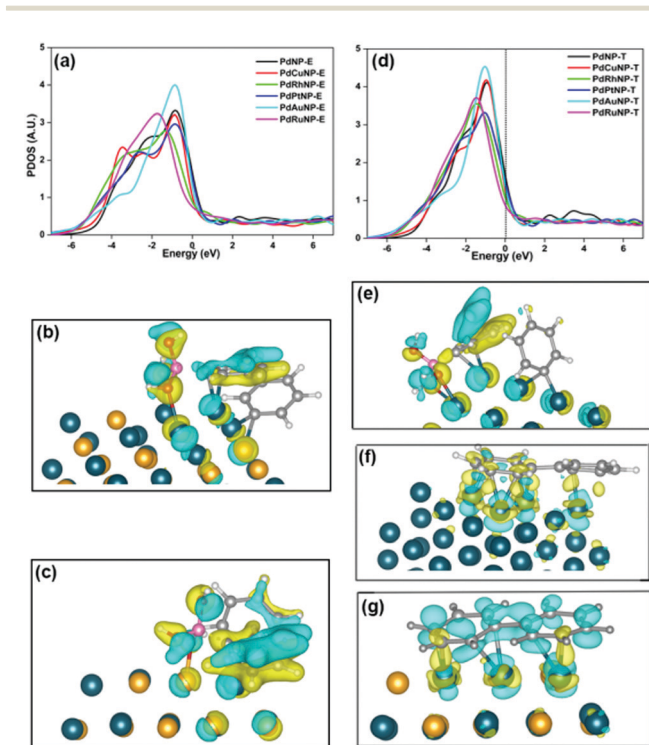


Fig. 8 (a and d) The PDOS of the Pd atoms at the top (right) and edge sites (left); the Fermi level is set to zero. (b), (c) and (e) Electron density difference plots for the transmetalation processes catalyzed by Pd₁₄₇ and Pd₇₄Cu₇₃ DENs; (b and c) represent phenylboronic acid adsorbed on Pd and Cu atoms on the surface of Pd₇₄Cu₇₃ DENs, whereas (e) represents the adsorption of phenylboronic acid on Pd₁₄₇ DENs. (f) and (g) Electron density difference plots for the adsorption of biphenyl on Pd₁₄₇ and Pd₇₄Cu₇₃ DENs; yellow contours represent charge accumulation, and green contours denote charge depression; cutoff = 0.002.

4. Conclusion

A series of Pd₇₄M₇₃ (M = Cu, Pt, Au, Rh, Ru) DENs were synthesized and their catalytic activities were investigated in Suzuki coupling reactions. Similar conversion rates for Suzuki coupling were observed for Pd₁₄₇ and Pd₇₄Cu₇₃ DENs, with HPLC yields of 79.9%/80.9% after 0.75 h reaction time, TONs of 6389/6546, and TOFs of 8519/8728 h⁻¹, respectively. DFT computations are helpful to elucidate the mechanism of the Suzuki coupling reaction and TOF. The calculated results indicate that although comparable energy barriers of the rate-determining step can be achieved by Pd₁₄₇ and Pd₇₄Cu₇₃ DENs, the adsorption energies of substrates on Pd₇₄Cu₇₃ DENs are slightly lower than those for Pd₁₄₇ DENs. The PDOS of top and edge Pd atoms and the electron density differences demonstrate that Cu synergizes with the Pd_x-Cu_{147-x} catalyst in the Suzuki coupling reaction. The Pd atoms facilitate the reaction process and act as a catalyst in the Suzuki cross-coupling reaction. In comparison, Cu atoms favor the transmetalation and desorption processes in the catalytic cycle. This work provides a general strategy for designing and synthesizing cheap bimetallic catalysts to boost the Suzuki coupling reaction.

Conflicts of interest

The authors declare no competing financial interest.

Acknowledgements

This work was supported by the National Key Research and Development Program of China (No. 2016YFC0906000 [2016 YFC0906003]), the National Natural Science Foundation of China (Grant No. 21573030), and Project of Chongqing Key Laboratory of Environmental Materials and Restoration Technology (CEK1803).

Notes and references

- M. Javier and J. R. Dunetz, *Chem. Rev.*, 2015, **46**, 2177–2250.
- N. Miyaura, *Chem. Rev.*, 2010, **36**, 41–123.
- Z. Zhang and Z. Wang, *J. Org. Chem.*, 2006, **71**, 7485–7487.
- G. Collins, M. Schmidt, C. O'Dwyer, G. McGlacken and J. D. Holmes, *ACS Catal.*, 2014, **4**, 3105–3111.
- M. Pérez-Lorenzo, *J. Phys. Chem. Lett.*, 2012, **3**, 167–174.
- Y. Li, E. Boone and M. A. El-Sayed, *Langmuir*, 2002, **18**, 4921–4925.
- N. T. Phan, M. Van Der Sluys and C. W. Jones, *Adv. Synth. Catal.*, 2006, **348**, 609–679.
- F. Heshmatpour, R. Abazari and S. Balalaie, *Tetrahedron*, 2012, **68**, 3001–3011.
- D. Astruc, L. Feng and J. R. Aranzas, *Angew. Chem., Int. Ed.*, 2005, **44**, 7852–7872.
- A. Balanta, C. Godard and C. Claver, *Chem. Soc. Rev.*, 2011, **40**, 4973–4985.
- S. W. Kim, M. Kim, W. Y. Lee and T. Hyeon, *J. Am. Chem. Soc.*, 2002, **124**, 7642–7643.
- Y. Yang, C. E. Castano, F. Gupton, A. C. Reber and S. N. Khanna, *Nanoscale*, 2016, **8**, 19564–19572.
- V. Farina, *Adv. Synth. Catal.*, 2004, **346**, 1553–1582.
- A. R. Siamaki, A. E. R. S. Khder, V. Abdelsayed, M. S. El-Shall and B. F. Gupton, *J. Catal.*, 2011, **279**, 1–11.
- Y. Yuan, A. C. Reber, S. E. Gilliland III, C. E. Castano and S. N. Khanna, *J. Catal.*, 2018, **360**, 20–26.
- C. C. C. Johansson Seechurn, M. O. Kitching, T. J. Colacot and V. Snieckus, *Angew. Chem., Int. Ed.*, 2012, **51**, 5062–5085.
- K. C. Nicolaou, P. G. Bulger and D. Sarlah, *Angew. Chem., Int. Ed.*, 2005, **44**, 4442–4489.
- S. Moussa, A. R. Siamaki, B. F. Gupton and M. S. El-Shall, *ACS Catal.*, 2012, **2**, 145–154.
- C. A. Fleckenstein and H. Plenio, *Chem. Soc. Rev.*, 2010, **39**, 694–711.
- Q. Fu, Y. Meng, Z. Fang, Q. Hu, L. Xu, W. Gao, X. Huang, Q. Xue, Y.-P. Sun and F. Lu, *ACS Appl. Mater. Interfaces*, 2017, **9**, 2469–2476.
- M. B. Thathagar, J. Beckers and G. Rothenberg, *J. Am. Chem. Soc.*, 2002, **124**, 11858–11859.
- Y. Yang, A. C. Reber, S. E. Gilliland, C. E. Castano, B. F. Gupton and S. N. Khanna, *J. Phys. Chem. C*, 2018, **122**, 25396–25403.
- T. Hatakeyama, T. Hashimoto, K. K. Kathriarachchi, T. Zenmyo, H. Seike and M. Nakamura, *Angew. Chem.*, 2012, **51**, 8834–8837.
- A. Fürstner, A. Leitner, M. Méndez and H. Krause, *J. Am. Chem. Soc.*, 2002, **124**, 13856–13863.
- S. D. Ramgren, L. Hie, Y. Ye and N. K. Garg, *Org. Lett.*, 2013, **15**, 3950–3953.
- M. Nasrollahzadeh, B. Jaleh and A. Ehsani, *Appl. Catal.*, 2015, **46**, 1148–1153.
- S. J. Kim, S.-D. Oh, S. Lee and S.-H. Choi, *J. Ind. Eng. Chem.*, 2008, **14**, 449–456.
- G. Schmid, D. C. A. Lehnert, J. O. Malm and J. O. Bovin, *J. Ind. Eng. Chem.*, 2010, **30**, 874–876.
- R. Ferrando, J. Jellinek and R. L. Johnston, *Chem. Rev.*, 2008, **108**, 845–910.
- B. Hammer and J. K. Nørskov, *Adv. Catal.*, 2000, **31**, 71–129.
- H. Xu, D. Cheng and Y. Gao, *ACS Catal.*, 2017, **7**, 2164–2170.
- H. Miura, Y. Tanaka, K. Nakahara, Y. Hachiya, K. Endo and T. Shishido, *Angew. Chem.*, 2018, **130**, 6244–6248.
- E. V. Carino, M. R. Knecht and R. M. Crooks, *Langmuir*, 2009, **25**, 10279–10284.
- S. V. Myers, A. I. Frenkel and R. M. Crooks, *Chem. Mater.*, 2009, **21**, 4824–4829.
- R. W. Scott, H. Ye, R. R. Henriquez and R. M. Crooks, *Chem. Mater.*, 2003, **15**, 3873–3878.
- J. M. Soler, E. Artacho, J. D. Gale, A. García, J. Junquera, P. Ordejón and D. Sánchez-Portal, *J. Phys.: Condens. Matter*, 2002, **14**, 2745.
- P. D. Dans, A. Crespo, D. A. Estrin and E. L. Coitiño, *J. Chem. Theory Comput.*, 2008, **4**, 740–750.
- S. D. Huang, C. Shang, P. L. Kang, X. J. Zhang and Z. P. Liu, *Wiley Interdiscip. Rev.: Comput. Mol. Sci.*, 2019, **9**, e1415.
- S. Huzinaga, *J. Chem. Phys.*, 1965, **42**, 1293–1302.
- T. H. Dunning Jr, *J. Chem. Phys.*, 1970, **53**, 2823–2833.
- J. P. Perdew, K. Burke and M. Ernzerhof, *Phys. Rev. Lett.*, 1996, **77**, 3865.
- B. Delley, *J. Chem. Phys.*, 1990, **92**, 508–517.
- S. Grimme, *J. Comput. Chem.*, 2006, **27**, 1787–1799.
- X.-J. Zhang and Z.-P. Liu, *J. Chem. Theory Comput.*, 2015, **11**, 4885–4894.
- X.-J. Zhang, C. Shang and Z.-P. Liu, *J. Chem. Theory Comput.*, 2013, **9**, 5745–5753.
- R. W. Scott, H. Ye, R. R. Henriquez and R. M. Crooks, *Chem. Mater.*, 2003, **15**, 3873–3878.
- M. R. Knecht, M. G. Weir, A. L. Frenkel and R. M. Crooks, *Chem. Mater.*, 2008, **20**, 1019–1028.
- M. Zhao, L. Sun and R. M. Crooks, *J. Am. Chem. Soc.*, 1998, **120**, 4877–4878.
- R. M. Anderson, Z. Liang, J. A. Loussaert, A. I. Frenkel, H. Graeme and R. M. Crooks, *ACS Nano*, 2013, **7**, 9345–9353.
- J. Rothe, J. Hormes, H. Bönnemann, W. Brijoux and K. Siepen, *J. Am. Chem. Soc.*, 1998, **120**, 6019–6023.
- Y.-M. Chung and H.-K. Rhee, *J. Mol. Catal. A: Chem.*, 2003, **206**, 291–298.
- R. W. Scott, O. M. Wilson, S.-K. Oh, E. A. Kenik and R. M. Crooks, *J. Am. Chem. Soc.*, 2004, **126**, 15583–15591.
- R. W. Scott, A. K. Datye and R. M. Crooks, *J. Am. Chem. Soc.*, 2003, **125**, 3708–3709.

- 54 M. G. Weir, M. R. Knecht, A. I. Frenkel and R. M. Crooks, *Langmuir*, 2010, **26**, 1137–1146.
- 55 Y.-M. Chung and H.-K. Rhee, *Catal. Lett.*, 2003, **85**, 159–164.
- 56 R. M. Anderson, D. F. Yancey, L. Zhang, S. T. Chill, G. Henkelman and R. M. Crooks, *Acc. Chem. Res.*, 2015, **48**, 1351–1357.
- 57 P. Kunal, H. Li, B. L. Dewing, L. Zhang, K. Jarvis, G. Henkelman and S. M. Humphrey, *ACS Catal.*, 2016, **6**, 4882–4893.
- 58 B. Lim, M. Jiang, P. H. Camargo, E. C. Cho, J. Tao, X. Lu, Y. Zhu and Y. Xia, *Science*, 2009, **324**, 1302–1305.
- 59 R. Bayan and N. Karak, *ACS Omega*, 2017, **2**, 8868–8876.
- 60 L. Bai, J.-X. Wang and Y. Zhang, *Green Chem.*, 2003, **5**, 615–617.
- 61 V. V. Namboodiri and R. S. Varma, *Green Chem.*, 2001, **3**, 146–148.
- 62 C. G. Blettner, W. A. König, W. Stenzel and T. Schotten, *J. Org. Chem.*, 1999, **64**, 3885–3890.
- 63 R. M. Anderson, D. F. Yancey, L. Zhang, S. T. Chill, G. Henkelman and R. M. Crooks, *Acc. Chem. Res.*, 2015, **48**, 1351–1357.
- 64 W. Tang, L. Zhang and G. Henkelman, *J. Phys. Chem. Lett.*, 2011, **2**, 1328–1331.
- 65 A. Bej, K. Ghosh, A. Sarkar and D. W. Knight, *RSC Adv.*, 2016, **6**, 11446–11453.
- 66 A. A. C. Braga, N. H. Morgon, G. Ujaque and F. Maseras, *J. Am. Chem. Soc.*, 2005, **127**, 9298–9307.
- 67 A. A. C. Braga, N. H. Morgon, G. Ujaque, A. Lledós and F. Maseras, *J. Organomet. Chem.*, 2006, **691**, 4459–4466.
- 68 B. Hammer, Y. Morikawa and J. K. Nørskov, *Phys. Rev. Lett.*, 1996, **76**, 2141–2144.
- 69 J. K. Nørskov, *Prog. Surf. Sci.*, 1991, **38**, 103–144.
- 70 A. Nilsson, L. G. M. Pettersson, B. Hammer, T. Bligaard, C. H. Christensen and J. K. Nørskov, *Catal. Lett.*, 2005, **100**, 111–114.
- 71 J. K. Nørskov, F. Abild-Pedersen, F. Studt and T. Bligaard, *Proc. Natl. Acad. Sci. U. S. A.*, 2011, **108**, 937–943.
- 72 B. Hammer and J. K. Nørskov, *Nature*, 1995, **376**, 238–240.